Macromolecules

ARTICLE

pubs.acs.org/Macromolecules

Crystallization and Melting of Poly(ethylene oxide) in Blends and Diblock Copolymers with Poly(methyl acrylate)

Dirk Pfefferkorn,[†] Samuel O. Kyerematen,[†] Karsten Busse,[†] Hans-Werner Kammer,[‡] Thomas Thurn-Albrecht,[†] and Jörg Kressler*[,†]

[†]Department of Chemistry and Physics, Martin Luther University Halle-Wittenberg, D-06099 Halle (Saale), Germany

[‡]Faculty of Applied Sciences, Universiti Teknologi MARA, 40450 Shah Alam/Selangor, Malaysia

Supporting Information

ABSTRACT: Blends of poly(ethylene oxide) (PEO) and poly(methyl acrylate) (PMA) as well as the respective diblock copolymers PEO-*b*-PMA form a homogeneous melt and undergo crystallization of PEO upon cooling. Although an identical PEO (M_n = 5000 g/mol) is used in blends and diblock copolymers, crystallization and melting behavior at comparable PMA contents differs strongly as revealed by temperature-resolved small-angle X-ray scattering (TR-SAXS) and differential scanning calorimetry (DSC) measurements. After isothermal crystallization, PEO lamellae in the blends thicken during heating from once-folded to extended chain crystals prior to melting as revealed by TR-SAXS. Contrarily, in PEO-*b*-PMA a thickening to extended chain lamellae is impossible when the PMA block exceeds an M_n of about 3000 g/mol. This behavior is caused by a balance between the tendency of the crystallizable block to form extended chain crystals, the tendency of the noncrystallizable chains to adopt a maximum in conformational entropy, and the space requirements of the these chains at the crystalline−amorphous interface. Thus, chain-folded crystals of PEO are formed as a compromise when the noncrystallizable chains become sufficiently long and can be considered to be in thermodynamic equilibrium. Equilibrium melting temperatures for neat PEO, T_m^0, and for PEO in blends and diblock copolymers, $T_{m,b}^0$, are determined using both the Hoffman−Weeks and the Gibbs−Thomson approach. Values determined by the Hoffman−Weeks method are generally lower compared to values obtained by the Gibbs−Thomson approach, which can be explained by inherent differences in extrapolation procedures. The maximum equilibrium melting point depression $T_m^0 - T_{m,b}^0$ is found to be 2 K in blends and 7 K in diblock copolymers. In the case of blends, melting point depression can be explained by Flory's entropy contribution of miscible polymer blends.

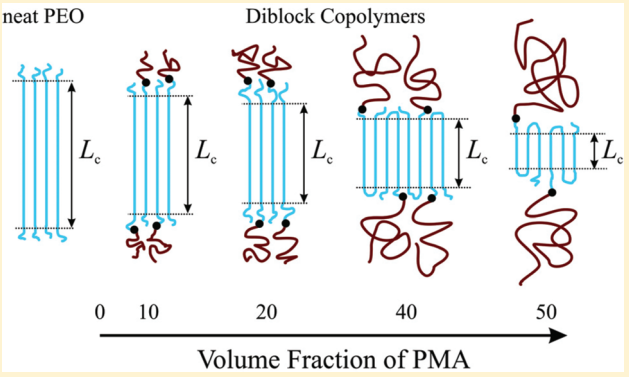

1. INTRODUCTION

Poly(ethylene oxide) (PEO) is miscible with various polymers[1] including poly(methyl acrylate) (PMA).[2,3] Thus, it is supposed that the corresponding diblock copolymers PEO-*b*-PMA possess also a disordered (single phase) melt. Using atom transfer radical polymerization (ATRP), PEO-*b*-PMA diblock copolymers are easily synthesized using monofunctional PEO macroinitiators. Accordingly, blends and diblock copolymers containing an identical PEO (except a small initiator fragment) can be prepared. This enables direct comparison of the crystallization and melting behavior of PEO in PEO/PMA blends as well as in PEO-*b*-PMA diblock copolymers.

The chemical potential of a repeat unit in the melt of a crystallizable polymer is reduced when miscible diluents are added. This results in a melting point depression (MPD) of the crystallizable polymer.[4] Hence, the MPD of miscible polymer blends has been studied widely and serves to deduce the Flory−Huggins interaction parameter χ from melting point data[5−7] according to a treatment established by Nishi and Wang.[8] In the past, various authors studied the crystallization of block copolymers having a crystallizable block from a microphase-separated melt. They reported melting temperatures which were remarkably lower than those of the corresponding homopolymers of similar molar mass.[9−15] The MPD in this case is caused by confinement of the crystallizable blocks into microphases restricting the extension of the polymer crystals. A detailed discussion about crystallization and melting in such block copolymers can be found elsewhere.[16−18] Furthermore, an MPD was also observed in block copolymers crystallizing from a disordered melt.[19−25] Thus, the question may arise whether there are differences in the melting and crystallization behavior between miscible binary polymer blends and their corresponding

Received: December 16, 2010
Revised: February 18, 2011
Published: March 16, 2011

diblock copolymers. As far as the authors know, there has not been any report in which melting and crystallization in miscible blends and diblock copolymers, both containing an identical crystallizable polymer of fixed molar mass and different amounts of a noncrystallizable polymer, have been analyzed systematically. It is the purpose of this study to compare melting and crystallization of PEO of number-average molar mass M_n = 5000 g/mol in blends with PMA as well as in diblock copolymers PEO-*b*-PMA over a wide range of composition. Investigations are carried out by means of differential scanning calorimetry (DSC) and temperature-resolved SAXS (TR-SAXS). The occurrence of a disordered melt in diblock copolymers is confirmed by TR-SAXS measurements. Equilibrium melting points are determined using both Hoffman−Weeks[26] and Gibbs−Thomson extrapolation approach.[27] The obtained results are compared and discussed. Furthermore, equilibrium melting temperatures serve to determine the MPD in both blends and diblock copolymers. The interaction parameter is deduced for blends, and the influence of the noncrystallizable block on the crystallization of PEO in the diblock copolymers is discussed.

2. THEORETICAL BACKGROUND

Because of the low melting temperature, small polydispersity, and the high degree of crystallinity achievable, low molar mass PEOs have been studied extensively in the past decades to gain a better understanding of polymer crystallization. It is thus well-known that PEO crystallizes at usual undercoolings exclusively with extended chains if the molar mass is sufficiently low ($M_n \leq$ 3000 g/mol)[28,29] or with chains folded n times (n being a small integer) for higher molar masses.[30−34] The fold number n is found to be a function of molar mass, crystallization temperature T_c, and crystallization time.[30−32] Additionally, lamellae with different fold numbers might be present in the same sample, especially at higher molar masses.[34−36] Although the extended chain crystal is thermodynamically favored, the folded chain crystals grow during isothermal crystallization due to kinetic reasons. Those folded chain crystals thicken in a stepwise manner to thermodynamically more stable states (smaller fold numbers or even extended chains) during heating. This lamella thickening in PEO has been studied by means of light microscopy,[37] DSC measurements,[38] and, more recently, TR-SAXS[39] and *in situ* AFM measurements.[40−42] PEO crystallizes in a 7_2 helix with a pitch of ∼1.95 nm.[43] Hence, the theoretical thickness of a lamella containing n-folded chains can be approximated as

$$L_c = \frac{1}{n+1}\frac{1.95}{7}N_2 \tag{1}$$

where N_2 is the degree of polymerization of PEO. In the following, indices 1 and 2 generally refer to the noncrystallizable and the crystallizable polymer, respectively. Note that eq 1 is somewhat simplified since it neglects the fact that several repeat units are necessary to form a fold and, thus, do not contribute to L_c. Furthermore, a crystalline structure with a chain tilting angle α would lead to a correction by cos α, which is not considered in this equation. Any tilting would therefore cause noninteger values of n.

Lamella thickening during heating has also been observed for numerous homopolymers, e.g., in polyethylene,[44] aliphatic polyamides,[45] poly(pivalolactone),[46] poly((*R*)-3-hydroxybutyrate),[47] or polylactide.[48] In homopolymers, folded chains are induced by kinetic reasons and thus represent a metastable state. Upon heating, the number of folds is reduced stepwise via lamella thickening. Hence, heating with an infinitely small heating rate would produce extended chain crystals. However, the situation is different for diblock copolymers where a noncrystallizable block is covalently bound to a crystallizable block and where both blocks are mutually miscible in the melt. From a thermodynamic point of view, the crystallizable block favors extended chains to reduce its free energy upon crystallization, whereas the noncrystallizable block tries to achieve a maximum of conformational entropy, i.e., the random coil conformation. Since both blocks are joined at the junction point, a completely extended crystalline chain would force the noncrystallizable chains to stretch drastically in order to retain bulk density, resulting in an enormous entropy penalty. This unfavorable situation can be avoided if the chains of the crystallizable block fold to some extent, thus creating a larger interfacial area between both blocks. That means crystallization from the homogeneous melt of such diblock copolymers is ruled by a balance between the two opposing tendencies, resulting in the formation of an equilibrium morphology where the noncrystallizable chains are somewhat stretched and the crystallizable chains are folded n times. The crystallization of diblock copolymers from a heterogeneous (i.e., microphase-separated) melt is theoretically treated by DiMarzio et al. using Gaussian chain statistics.[49] Assuming a lamellar morphology, they found that crystalline lamella thickness L_c and the thickness of the amorphous layer L_a between two lamellae scale with the length of both blocks according to the scaling laws

$$L_c \propto N_2 {N_1}^{-1/3} \tag{2}$$

$$L_a \propto {N_1}^{2/3} \tag{3}$$

where N_1 and N_2 are the degrees of polymerization of noncrystallizable and crystallizable blocks, respectively. The corresponding scaling law for the long period $d \equiv L_c + L_a$ is $d \propto N{N_1}^{-1/3}$, where $N \equiv N_1 + N_2$. Using the mean-field approximation, Whitmore and Noolandi[50] obtained analogue relations, which differ only in exponents: −5/12 in eq 2 and 7/12 in eq 3. In both theories, it is predicted that the fold number n increases with increasing length of the noncrystallizable block. Both theories have been tested for diblock copolymers containing the two incompatible blocks PEO and poly(*tert*-butyl methacrylate).[10] It has been found that the experimentally observed scaling of L_c and L_a with N_1 is in moderate agreement with the theoretical scaling laws. In addition, Lee and Register[23] tested the scaling law on diblock copolymers containing compatible blocks. They determined long periods d of crystallized diblock copolymers with fixed length of the crystallizable block and varying length of the noncrystallizable block. They found that d follows the scaling law $d \propto N{N_1}^{-1/3}$ to a good approximation. Thus, the theories seem to be applicable for crystallization of diblock copolymers from both heterogeneous and homogeneous melts.

Since crystallization of polymers occurs usually far away from thermodynamic equilibrium (large undercooling), one has to rely on extrapolation methods for the determination of equilibrium melting temperatures T_m^0. In numerous reports it has been shown that the experimentally observed melting temperature T_m of polymers is a function of the crystallization temperature T_c. Thus, Hoffman and Weeks[26] derived the relationship

$$T_m = \alpha T_c + (1-\alpha)T_m^0 \tag{4}$$

where α is related to a slight thickening of an isothermally grown lamella. If α = constant, the relationship is linear, and a linear extrapolation of a plot of T_m vs T_c to the equilibrium line given by $T_m = T_c$ yields T_m^0. Owing to its experimental simplicity, this procedure has been widely used to determine T_m^0. But, also nonlinear relationships have been observed,[51−53] which render an unambiguous extrapolation difficult. Hence, attempts have been made to refine the approach, at the expense of its simplicity.[51,54] Moreover, in recent publications doubts have been cast on the general validity of this approach.[55−60]

It is a well established fact that the melting temperature is a function of the crystal thickness, i.e.

$$T_m = T_m^0\left(1 - \frac{B}{L_c}\right) \quad (5)$$

where L_c is the lamella thickness and $B \equiv 2\gamma V_c/\Delta H_m^0$, with γ being the surface free energy of the interface between the crystal and the surrounding liquid, V_c the molar volume of a crystallizable repeat unit, and ΔH_m^0 the enthalpy of melting (per mole of crystalline units) of a 100% crystalline polymer of high molar mass. Equation 5 determines the depression of the equilibrium melting temperature being caused by unfavorable contributions of the fold surface in crystals of finite size. Of course, ΔH_m^0 will be reduced due to the presence of chain ends or chain folds in the crystalline/amorphous interface.[61] However, the influence is small and thus this contribution will be neglected. Equation 5 is usually referred to as the Gibbs−Thomson equation in polymer literature, which has also been modified.[62−66] Important is the fact that eq 5 provides another method to determine T_m^0: it can be obtained by extrapolating a plot of T_m (e.g., determined from DSC experiments) vs reciprocal lamella thickness (measured by SAXS) to zero. Lamella thickness and melting temperature might also be simultaneously obtained in the X-ray device, but it can be assumed that the temperature control in the DSC device is more accurate. However, the experimental effort for the Gibbs−Thomson method is much higher compared to the Hoffman−Weeks approach, and the extrapolated value of T_m^0 might be seriously influenced by experimental conditions such as heating rate and lamellae thickness distribution.[67]

At equilibrium between a crystal and its melt, the chemical potentials of both phases must be equal, i.e., $\mu_2^c = \mu_2^l$. This equality is satisfied at T_m^0. If a miscible, low-molar-mass diluent is added, the chemical potential of the melt decreases whereas that of the crystal remains unchanged, supposing that no diluent molecules are incorporated into the crystal. As a consequence, the equilibrium condition is satisfied at a lower temperature $T_{m,b}^0$, the equilibrium melting temperature of the crystalline polymer in the mixture. For the particular case of polymer−diluent mixtures, Flory derived an expression for the resulting MPD.[4] The corresponding expression for miscible binary polymer blends reads[8]

$$\frac{1}{T_{m,b}^0} - \frac{1}{T_m^0} = -\frac{R}{\Delta H_m^0}\frac{V_2}{V_1}(A + \chi\varphi_1^2) \quad (6)$$

where φ_1 is the volume fraction of the noncrystallizable component, V_i are the molar volumes of the segments of component i, and χ is the Flory−Huggins interaction parameter. Quantity A is essentially an entropy-related term and for miscible binary blends given by $A = [\ln(1 - \varphi_1)]/N_2 + \varphi_1(1/N_2 - 1/N_1)$, but this contribution is usually neglected if the degrees of polymerization are high. Equation 6 has been widely used to deduce the χ-parameter for melt-miscible blends. However, it cannot be applied to diblock copolymers.

Table 1. Molar Mass Data of the Polymers, Degree of Polymerization N_1 of the PMA, and PMA Volume Fraction φ_1 of the Synthesized Diblock Copolymers

polymer	M_n[a] (g/mol)	M_w/M_n[b]	N_1	φ_1[c]
PEO	5000	1.03		
PEO-*b*-$PMA_{7.7}$	5690	1.03	6	0.077
PEO-*b*-$PMA_{14.3}$	6210	1.05	12	0.143
PEO-*b*-$PMA_{32.7}$	8190	1.08	35	0.327
PEO-*b*-$PMA_{37.9}$	8970	1.08	44	0.379
PEO-*b*-$PMA_{53.8}$	12410	1.15	84	0.538
PEO-*b*-$PMA_{73.9}$	22740	1.22	204	0.739
PMA	5400	1.35	63	

[a] Calculated from ^{1}H NMR spectrum. [b] Determined by SEC using THF/dimethylacetamide (90 vol % THF) as eluent and PMMA standards. For the homopolymers THF was used as eluent and PEO and PMMA standards, respectively. [c] Calculated according to Flory's definition using segment molar masses which have been reported in ref 3. See Supporting Information for details.

3. EXPERIMENTAL SECTION

3.1. Materials and Synthesis. PEO and PMA homopolymers used in this study were the same as those reported previously.[3] PEO was terminated by one hydroxyl and one methoxy end group. Number-average molar masses M_n of the homopolymers were calculated using ^{1}H NMR spectra. The polydispersity index M_w/M_n was determined by size exclusion chromatography (SEC) using tetrahydrofuran (THF) and PEO and poly(methyl methacrylate) (PMMA) standards. Table 1 lists the characteristic data of the homopolymers. PEO-*b*-PMA diblock copolymers with varying PMA block lengths were synthesized using atom transfer radical polymerization (ATRP) in anisole with CuBr as catalyst, 2,2′-bipyridine as ligand, and PEO as macroinitiator. CuBr (99%, Fluka) was purified by excessive washing with glacial acetic acid, rinsed with absolute ethanol, and dried overnight in a vacuum oven at 80 °C. Dichloromethane (99.8%, Aldrich), 2-bromoisobutyryl bromide (BIB) (98%, Aldrich), and 2,2′-bipyridine (bipy) (99.5%, Merck) were used as received. Methyl acrylate (MA) (99%, Aldrich), anisole (99%, Alfa Aesar), and triethylamine (TEA) (99.5%, Fluka) were dried over CaH_2 and then distilled under vacuum. THF and diethyl ether were dried over potassium hydroxide and distilled before use. The PEO macroinitiator (PEO-Br) was synthesized by esterification of the hydroxyl group of the PEO with BIB as follows: 15 g of PEO (3 mmol) was dissolved in 100 mL of dry dichloromethane, and then 0.9 mL of freshly distilled TEA (6 mmol) was added to the solution. The flask was immersed in an ice bath, and 0.75 mL of BIB (6 mmol) was slowly added within 1 h. The reaction was allowed to proceed at room temperature for 24 h. Then the solvent was removed by rotary evaporation, and the crude product was redissolved in THF. The solution was allowed to stand overnight to precipitate the TEA hydrobromide, which was filtered off as white, needlelike crystals. Further purification was achieved by passing the solution through a silica column. The purified solution was precipitated into cold diethyl ether and dried in vacuum for 2 days. In a typical ATRP procedure, appropriate amounts of CuBr and bipy were placed in a dry Schlenk flask equipped with a stir bar. The molar ratio of CuBr to bipy was set to 1:2. The flask was sealed with a rubber septum and was evacuated and backfilled with nitrogen three times, before degassed anisole was introduced via a nitrogen-purged syringe. The mixture was stirred under continuous nitrogen purge until a homogeneous solution was obtained. This was followed by the addition of appropriate amounts of degassed methyl acrylate with a nitrogen-purged syringe. The macroinitiator PEO-Br was dissolved separately in a small amount of anisole. This solution was degassed and added to the reaction

mixture via a syringe. Then the whole solution was subjected to three freeze−thawing cycles. After this treatment the flask was immersed in an oil bath (85 °C), and the reaction was allowed to proceed overnight under a nitrogen atmosphere. Finally, the solution was diluted with THF, passed through a silica column to remove the catalyst complex, and precipitated into cold diethyl ether. The precipitate was washed with an excess of diethyl ether/acetone (10 vol % acetone) to remove possibly formed PMA homopolymer, followed by drying under vacuum for 3 days. Composition of the diblock copolymers was determined using ^{1}H NMR spectra. The spectra indicate that the diblock copolymers did not contain any unreacted macroinitiator. Characteristic data of the diblock copolymers are listed in Table 1. In the following, diblock copolymers will be denoted by PEO-*b*-PMA*x* and blends by PEO/PMA*x*. In both cases, *x* refers to the PMA content in volume percent.

PEO/PMA blends with PMA contents of 10−50 wt % (in increments of 10 wt %) were prepared by dissolving the homopolymers in dichloromethane. The solvent was evaporated, and the samples were dried for 24 h at 80 °C under vacuum. Blends and diblock copolymers were isothermally crystallized at various crystallization temperatures T_c ranging from 25 to 45 °C. For this purpose, the samples were heated to 80 °C and annealed for 15 min in order to remove any residual solvent and to facilitate homogenization of the melt. Subsequently, the samples were quenched to the respective T_c and isothermally crystallized for 24 h. The crystallization process was conducted on hot stages having a temperature accuracy of ±0.1 K.

3.2. Differential Scanning Calorimetry. Differential scanning calorimetry (DSC) experiments were performed under continuous nitrogen flow using a Mettler Toledo DSC 823e module. Aluminum pans were filled with about 10 mg of sample. Isothermally crystallized samples were heated from T_c to 80 °C at a heating rate of 0.5 K/min. DSC traces were baseline-corrected. The maximum of the endothermal peak was taken as the melting temperature T_m, and the specific melting enthalpy $\Delta\tilde{H}_m$ was obtained from integration of the endothermal peak. The determined melting temperatures were plotted as a function of crystallization temperature T_c. Equilibrium melting temperatures were obtained by extrapolating data to $T_m = T_c$ according to the procedure outlined by Hoffman and Weeks.[26]

3.3. TR-SAXS Measurements. Temperature-resolved small-angle X-ray scattering (TR-SAXS) measurements were performed with Cu Kα radiation emitted from a Rigaku Rotaflex rotating anode with pinhole collimator. Isothermally crystallized samples were transferred as fast as possible to a Linkam hot stage located in the SAXS chamber and were immediately reheated to the respective crystallization temperature. In order to follow morphology changes during heating, the TR-SAXS measurements were performed from T_c to T_m in steps of 1 K. The time necessary to acquire a good scattering trace varied from a minimum of 120 s up to 300 s, depending on the PMA content. After a measurement was completed, the temperature was raised slowly by 1 K with a heating rate of 1 K/min. Thus, the average heating rate varied between 0.1 and 0.4 K/min. The cycle was repeated until the sample was completely molten, as indicated by the absence of any reflection. Recorded SAXS intensities were corrected for background scattering, and the one-dimensional correlation function was calculated by cosine Fourier transformation. The correlation function served to extract long period d as well as lamella thickness L_c according to the standard procedure.[68] The accuracy of determined L_c values was estimated to be ±6 Å. L_c was determined both directly after isothermal crystallization and from the last evaluable SAXS curve before melting. The latter value was correlated to the T_m obtained from DSC. This treatment is different from that of Strobl,[55−60] who determines L_c and T_m simultaneously in the SAXS device. However, in the present study it is found that T_m obtained from DSC measurements is in good agreement with the temperature of the onset of melting observed in the SAXS experiments.

4. RESULTS AND DISCUSSION

4.1. DSC Measurements. DSC traces of PEO/PMA blends, obtained with a heating rate of 0.5 K/min, possess a single melting peak which slightly shifts to lower temperatures with increasing PMA content (Figure 1a). If a much higher heating rate of 5 K/min is used, bimodal DSC traces are observed. This is due to the presence of crystals with different fold numbers; i.e., fast heating prevents a complete unfolding of the PEO from an initial, more-folded state to a final, less-folded state. This can be avoided by slowly heating with 0.5 K/min as can be seen in Figure 1. The tiny shoulders at the lower-temperature tail indicate the presence of only a small fraction of the more-folded chain crystals. The degree of crystallinity X_{DSC} is calculated from $X_{DSC} = \Delta\tilde{H}_m/\Delta\tilde{H}^0_m$, where $\Delta\tilde{H}_m$ is the specific enthalpy of melting of the samples and $\Delta\tilde{H}^0_m = 197$ J/g is the specific enthalpy of melting of 100% crystalline extended chain PEO crystals.[69] DSC traces of diblock copolymers show also single melting peaks which shift stronger to lower temperatures with increasing PMA content (Figure 1b). Additionally, a DSC trace of PEO-*b*-PMA$_{73.9}$, crystallized at 25 °C for 30 days, is also included in Figure 1b to illustrate the influence of the PMA block length on melting temperature. T_m and X_{DSC} of blends and diblock copolymers crystallized at 40 °C are listed in Table 2. Additionally, values of the fractional crystallinity X'_{DSC} of the PEO, which is calculated from X_{DSC} divided by the PEO weight fraction w_2, are included in Table 2 for both blends and diblock copolymers.

4.2. TR-SAXS Measurements. Flexible semicrystalline polymers consist usually of isotropically arranged stacks of lamellae in which the lamellae are separated by amorphous layers; i.e., a periodic structure of separated regions with high and low electron density is formed. Of course, this is an simplified picture, and a considerably extended interphase might be taken into account which results in a three-phase model.[70] When the dimension of the stacks is large compared to the long period d, the scattering behavior of such a system can be related to the electron density distribution via the one-dimensional electron density correlation function $K(z)$, which is defined as

$$K(z) = \frac{1}{8\pi^3 r_e^2}\int_0^\infty 4\pi q^2 I(q)\cos(zq)\,dq \qquad (9)$$

where r_e is the classical electron radius, q the scattering vector, $I(q)$ the scattering cross section, and z the direction along the normal to the lamella surface.[68] The characteristic shape of this function allows the determination of long period and lamella thickness as illustrated in Figure S1 of the Supporting Information. Figure 2a shows the results of TR-SAXS measurements of neat PEO. Initially, at 40 °C a peak at $q^* = 0.39$ nm^{-1}, corresponding to a long period d of 16.1 nm, and its second and third orders are observed. The high degree of crystallinity of $X_{DSC} = 0.86$ allows for unambiguous distinction between the lamella thickness L_c and the thickness of the amorphous layer L_a. The L_c value is found to be 14.7 nm. With the long period of 16.1 nm it results in a thickness of the amorphous layer of 1.4 nm. Thus, the degree of crystallinity obtained from SAXS data is 0.91, which is in good agreement with the value of 0.86 obtained by DSC. According to eq 1, the theoretical length of a once-folded PEO chain with a degree of polymerization of $N_2 = 114$ amounts to ∼16 nm. Thus, it might be concluded, within experimental error of data evaluation of nonperfect correlation function (i.e., as in most cases[68] the correlation triangle is not perfectly observed),

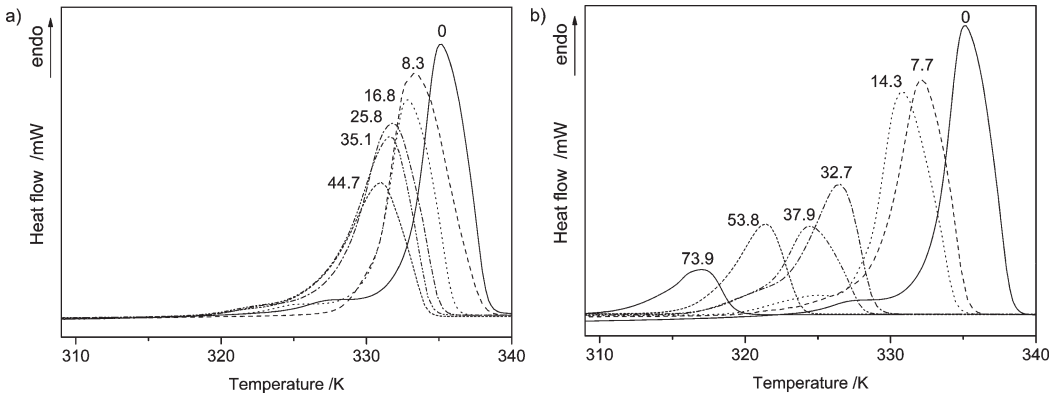

Figure 1. DSC traces of (a) PEO/PMA blends and (b) PEO-*b*-PMA diblock copolymers obtained from a heating run with a rate of 0.5 K/min. Samples were isothermally crystallized at 40 °C for 24 h except PEO-*b*-PMA$_{73.9}$, which was crystallized at 25 °C for 30 days. Numbers at the traces indicate the PMA content of the samples in volume percent.

Table 2. Melting Temperature T_m, Specific Enthalpy of Melting $\Delta\tilde{H}_m$, Degree of Crystallinity X_{DSC}, and Fractional Crystallinity of PEO X'_{DSC} of Blends and Diblock Copolymers[a]

blends	T_m (K)	$\Delta\tilde{H}_m$ (J/g)	X'_{DSC}[b]	X'_{DSC}[c]	copolymers	T_m (K)	$\Delta\tilde{H}_m$ (J/g)	X_{DSC}[b]	X'_{DSC}[c]
PEO	335.3	169	0.86		PEO-*b*-PMA$_{7.7}$	332.2	134	0.68	0.75
PEO/PMA$_{8.3}$	333.3	156	0.79	0.88	PEO-*b*-PMA$_{14.3}$	331.0	116	0.59	0.71
PEO/PMA$_{16.8}$	333.0	120	0.61	0.76	PEO-*b*-PMA$_{32.7}$	326.4	81	0.41	0.66
PEO/PMA$_{25.8}$	331.9	112	0.57	0.81	PEO-*b*-PMA$_{37.9}$	324.5	73	0.37	0.65
PEO/PMA$_{35.1}$	331.6	91	0.46	0.77	PEO-*b*-PMA$_{53.8}$	321.5	45	0.23	0.56
PEO/PMA$_{44.7}$	331.2	71	0.36	0.72	PEO-*b*-PMA$_{73.9}$[d]	317.3	28	0.14	

[a] Values are determined by DSC measurements using a heating rate of 0.5 K/min. Samples were isothermally crystallized for 24 h at 40 °C. [b] Calculated from $X_{DSC} = \Delta\tilde{H}_m/\Delta\tilde{H}^0_m$ using $\Delta\tilde{H}^0_m = 197$ J/g.[69] [c] Fractional crystallinity $X'_{DSC} = X_{DSC}/w_2$, where w_2 is the weight fraction of PEO. [d] Because of low melting temperature and very slow crystallization, this sample was crystallized at 25 °C for 30 days.

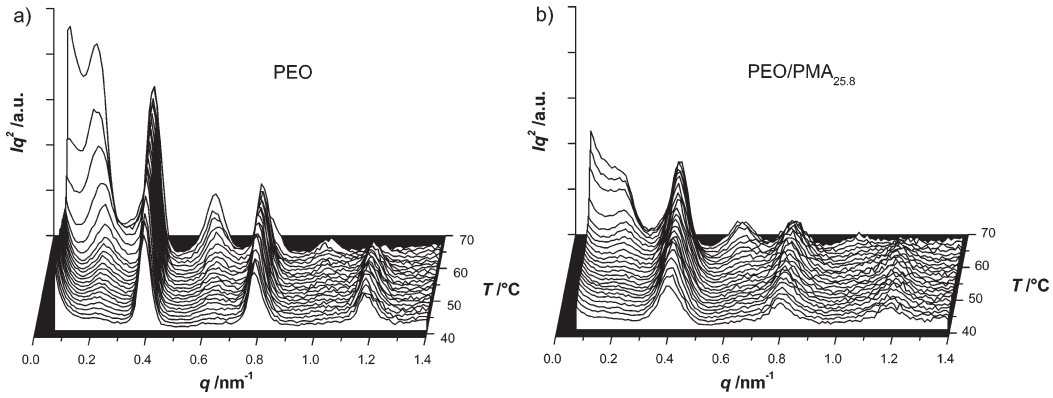

Figure 2. Evolution of Lorentz-corrected SAXS intensity profiles during heating from 40 °C to the beginning of the melting process: (a) neat PEO and (b) PEO blended with 25.8 vol % PMA. Samples were isothermally crystallized for 24 h at 40 °C.

that once-folded PEO chain crystals grow during isothermal crystallization at 40 °C. Upon heating, a second peak appears at $q^* = 0.21$ nm^{-1} ($d = 28.6$ nm), indicating the formation of extended chain crystals. This peak rapidly grows in intensity and slightly shifts to $q = 0.19$ nm^{-1} shortly before melting, which corresponds to a long period of $d = 33$ nm. From the correlation function a lamella thickness of $L_c = 29.8$ nm is obtained. Since the theoretical length of a fully extended PEO chain with $N_2 = 114$ amounts to $L_{c,max} = 32$ nm according to eq 1, it can be concluded that this peak originates from extended chain crystals. Crystallinity does not change significantly during heating, which indicates a complete recrystallization or lamella thickening. The TR-SAXS results clearly reveal that during heating once-folded chain crystals thicken to extended chain crystals. The observed behavior is in full agreement with data reported by Tang et al. for a PEO of identical molar mass.[39]

The blends behave similarly as neat PEO. Figure 2b shows an example of TR-SAXS traces for the blend PEO/PMA$_{25.8}$ isothermally crystallized at 40 °C. For long period d and lamella thickness L_c, both determined near the melting temperature, it is

found that d increases slightly with increasing amount of PMA in the blend whereas L_c shows minor decrease (Table 3). Without chain tilting, the ratio between actual lamella thickness L_c and maximum crystal thickness $L_{c,max}$ corresponds to the amount of crystalline units per PEO chain; the remaining units thus form dangling chain ends. Assuming that only chain tilting occurs, this ratio corresponds to the cosine of the tilt angle. (Because of the observed lengths, no chain folding exists here.) Of course, both situations are ideal, and it is rather likely that the observed behavior of L_c is actually caused by a combination of the two effects. In both cases, the obtained ratios are significantly larger than the corresponding fractional DSC crystallinities X'_{DSC}. This difference indicates the amount of PEO chains being completely dissolved in the amorphous state. In case of blends, between 6 and 17% of all PEO chains are not involved in a crystalline structure. The amorphous layer between two crystalline lamellae consists therefore of the remaining amorphous PEO units (cilia) of the partially crystallized PEO chain and an amorphous PEO/PMA mixture. The relative amount of PMA molecules in this layer can be calculated from the measured long period and leads to a continuous increase from 3% to 18% per partially crystallized PEO chain with increasing PMA content of the blend. The amount of PEO chains remaining in the PMA matrix is therefore of the same order as the amount of PMA chains in the amorphous layer between two PEO crystal lamellae.

The TR-SAXS measurements on PEO-*b*-PMA$_{7.7}$ (Figure 3a) indicate a different melting behavior compared to neat PEO and the PEO/PMA blends. Initially, only two peaks appear at q^* = 0.336 nm^{-1} (d = 18.7 nm) and q = 0.68 nm^{-1} after crystallization at 40 °C, corresponding to the first- and second-order reflection of long periods including a once-folded chain crystal. The initial lamella thickness after isothermal crystallization is L_c = 13 nm, which is close to the theoretical value of a once-folded PEO chain of 16.0 nm. The most interesting point is that additional peaks, which could be assigned to extended chain crystals, do not appear during heating. Instead, q^* shifts continuously to 0.171 nm^{-1} prior to melting, which corresponds to a long period of d = 36.7 nm. Analysis of the correlation function yields a lamella thickness of L_c = 26.2 nm. Thus, the majority of the PEO blocks forms extended chain crystals prior to melting. The somewhat smaller dimension compared to the theoretical value of 32 nm might be caused by the presence of a small amount of once-folded chain crystals or crystal imperfections as will be discussed below. The crystallinity calculated from the SAXS data is 0.71, which is in good agreement with the value of 0.68 obtained from DSC measurement (see Table 2). For PEO-*b*-PMA$_{14.3}$, the results are very similar (Figure S2, Supporting Information), except that the first peak appears at a lower scattering vector of q^* = 0.316 nm^{-1} (d = 19.9 nm). This peak shifts continuously to a final value of 0.174 nm^{-1} (d = 36.1 nm) close to the melting temperature. The third-order peak appears at q = 0.93 nm^{-1}, but the second-order peak has a very low intensity. Hence, it can be assumed that lamella thickness L_c and amorphous thickness L_a in this sample are quite similar because a second-order reflection can only vanish when both thicknesses are identical, i.e., when the lamellar structure is symmetric.[71−73] In such a case, determination of L_c from the correlation function alone is not reliable. A reasonable result of L_c is obtained using X_{SAXS} = 0.58, which is in good agreement with the DSC results. Initial lamella thickness after crystallization is found to be 11.5 nm, whereas the lamella thickness close to the melting point is ∼21 nm. The latter length is more than a once-folded but less than a completely extended PEO chain. Possible reasons for this observation will be discussed below.

After isothermal crystallization at 40 °C of sample PEO-*b*-PMA$_{32.7}$ (Figure 3b), one observes a peak at q^* = 0.275 nm^{-1} (d = 22.8 nm) and two higher order reflections at approximately 0.55 and 0.82 nm^{-1}. An initial lamella thickness of ∼9 nm after isothermal crystallization is obtained from the correlation function. According to eq 1, this is in the range of twice-folded PEO chains (L_c = 10.7 nm for N_2 = 114). During heating to the melting temperature, a continuous shift of q^* toward a value of 0.164 nm^{-1} (d = 38.3 nm) is observed. This yields a final lamella thickness of L_c = 15 nm corresponding to a once-folded PEO chain. One may conclude that PEO in PEO-*b*-PMA$_{32.7}$ thickens from twice to once-folded chain lamellae during heating, but further thickening to extended chains lamellae does not occur. The TR-SAXS traces of PEO-*b*-PMA$_{37.9}$, isothermally crystallized at 40 °C, show a very similar behavior (Figure S3,

Table 3. Long Period d, Lamella Thickness L_c, and SAXS Crystallinity $X_{SAXS} = L_c/d$ of Blends and Diblock Copolymers[a]

blends	d (nm)	L_c (nm)	X_{SAXS}	copolymers	d (nm)	L_c (nm)	X_{SAXS}
PEO	33.1	29.8	0.90				
PEO/PMA$_{8.3}$	34.0	29.8	0.87	PEO-*b*-PMA$_{7.7}$	36.7	26.2	0.71
PEO/PMA$_{16.8}$	34.3	29.4	0.86	PEO-*b*-PMA$_{14.3}$	36.1	20.9	0.58
PEO/PMA$_{25.8}$	36.1	27.8	0.77	PEO-*b*-PMA$_{32.7}$	38.3	15.0	0.39
PEO/PMA$_{35.1}$	37.9	26.2	0.69	PEO-*b*-PMA$_{37.9}$	39.5	12.8	0.32
PEO/PMA$_{44.7}$	38.3	26.6	0.70	PEO-*b*-PMA$_{53.8}$	44.5	10.0	0.22

[a] Values are determined from SAXS traces recorded prior to melting. Samples were isothermally crystallized at 40 °C for 24 h.

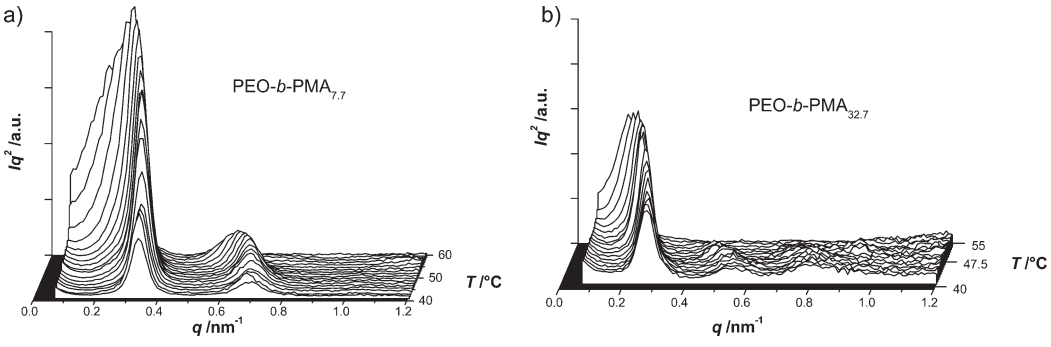

Figure 3. Evolution of Lorentz-corrected SAXS intensity profiles during heating from 40 °C to the beginning of the melting process: (a) PEO-*b*-PMA$_{7.7}$ and (b) PEO-*b*-PMA$_{32.7}$. Samples were isothermally crystallized for 24 h at 40 °C.

Supporting Information), but with the first peak appearing at $q^* = 0.266\ nm^{-1}$ ($d = 23.6$ nm). Prior to melting, a long period $d = 39.5$ nm and a lamella thickness $L_c = 12.8$ nm are obtained, i.e., the chains are once-folded. The first-order reflection of the diblock copolymer PEO-*b*-$PMA_{53.8}$ is observed at $q^* = 0.193\ nm^{-1}$ ($d = 32.6$ nm). It approaches a value of $0.141\ nm^{-1}$ ($d = 44.5$ nm) close to the melting temperature. A calculated lamella thickness of 10 nm was obtained for the diblock copolymer PEO-*b*-$PMA_{53.8}$ correlating with a twice-folded state of the PEO chains close to the melting point. Additionally, SAXS measurements are performed on the diblock copolymer with the longest PMA block, PEO-*b*-$PMA_{73.9}$, which was crystallized at 25 °C for 30 days. Because of the low melting temperature (see Table 2), this sample could not be crystallized at 40 °C. The first peak in the SAXS trace appears at $q^* = 0.12\ nm^{-1}$ ($d = 52.4$ nm), but no higher-order peaks are observed. Unfortunately, during heating q^* exceeds the resolution of the SAXS device, preventing determination of final L_c. Long period d and lamella thickness L_c of each diblock copolymer are listed in Table 3. It can be seen that d increases remarkably with increasing length of the amorphous PMA block whereas L_c decreases.

Considering the crystallization in melt-miscible blends of a crystallizable and a noncrystallizable polymer, the final morphology is strongly influenced by the behavior of the noncrystallizable component. Two extreme cases may be distinguished: (i) during crystallization the noncrystallizable polymer is completely incorporated into the amorphous layers between the lamellae, resulting in an increase of the long period that scales with the volume fraction of the noncrystallizable polymer, and (ii) the noncrystallizable polymer is fully excluded from the amorphous layer between the lamellae, resulting in a nearly unchanged long period for all blend ratios. If full exclusion of the noncrystallizable component occurs, it is thus expected that the SAXS crystallinity $X_{SAXS} \equiv L_c/d$ remains almost constant, provided that L_c does not alter significantly with blend composition. Localization of the noncrystallizable component is mainly influenced by competition between crystal growth rate R_c and diffusion rate R_d of the noncrystallizable component away from the crystal growth front. If $R_c > R_d$, the noncrystallizable polymer is trapped between growing lamellae during crystallization. If $R_c < R_d$, the noncrystallizable polymer has sufficient time to diffuse away from the crystal growth front and (partial) exclusion will be observed. It has been shown that this simple relationship holds when the polymer interactions are weak; i.e., in this case localization of the noncrystallizable polymer is only ruled by its mobility (i.e., by its glass transition temperature).[74] Strong interactions between both polymer species may lead to a more complex situation.[74−76] A (partial) exclusion of the noncrystallizable polymer has been observed in miscible blends of PEO and poly(vinyl acetate)[74,77,78] and of isotactic and atactic polystyrene.[79] In contrast, inclusion of the noncrystallizable component in the lamella stacks has been reported for miscible PEO/PMMA,[74,80] poly(vinyl chloride)/poly(ε-caprolactone) (PCL),[81] and PCL/poly(styrene-*co*-acrylonitrile) blends.[82] As mentioned above, the long period d in PEO/PMA blends, as determined close to melting temperature, increases slightly with increasing amount of PMA (Table 3). In addition, only a slight decrease of L_c with increasing PMA content is observed (Table 3). Crystallinities X_{DSC} and X_{SAXS} for the blends are plotted in Figure 4a as a function of PEO weight fraction. One observes a strong decrease of X_{DSC}, whereas X_{SAXS} shows only a minor decrease. Since SAXS probes only the lamella stacks, these results point toward partial exclusion of the PMA. Further evidence arises from the fact that the fractional crystallinity X'_{DSC} of the PEO in the blends is found to be in good agreement with X_{SAXS} (see Figure 4a). From crystallinity values X_{DSC} and X_{SAXS}, the weight fraction of excluded PMA can be estimated. It is found to increase linearly with increasing PMA content. The exclusion of the PMA is caused by its low glass transition temperature ($T_g = 10$ °C),[3] resulting in a large chain mobility at the crystallization temperature of 40 °C, and a χ-parameter between PEO and PMA being only very small negative as discussed below. However, in diblock copolymers, the situation is entirely different. Because of the covalent link between both blocks, a diffusion of PMA away from the growth front is not possible. Thus, one would expect that PMA is nearly completely included in the amorphous layers between the lamellae. A comparison of X_{DSC} and X_{SAXS} reveals that both values are in good agreement (Figure 4b), indicating that the majority of the PMA indeed remains in the amorphous layer between the lamellae as expected. The weight fraction of excluded PMA is negligible compared to the blends.

From the L_c values of diblock copolymers with different PMA block length it can be concluded that the PEO block in PEO-*b*-$PMA_{7.7}$ and PEO-*b*-$PMA_{14.3}$ adopts mainly an extended chain conformation close to the melting point, but with lengths being less than the theoretical value of 32 nm. This behavior is probably due to chain tilting. Alternatively, the influence of the covalently connected amorphous block might hamper a full extension of the PEO chain due to steric reasons. A complete extension of the PEO chains would require a sharp interface between the crystalline and the amorphous regions. To avoid such a sharp transition, several repeat units of those PEO chain ends which are connected to the amorphous block do not crystallize; i.e., they are not part of the crystal but contribute to the interphase. TR-SAXS data furthermore reveal that the PEO chains in PEO-*b*-$PMA_{32.7}$ and PEO-*b*-$PMA_{37.9}$ are once-folded prior to melting, whereas those in PEO-*b*-$PMA_{53.8}$ are twice-folded. Hence, it becomes clear that above a certain PMA block length the PEO chains can no longer unfold to extended chains during heating below the melting temperature due to the influence of the PMA block. Complete unfolding of the PEO block would lead to an enormous stretching of the PMA chains and thus to an entropy penalty. This is counterbalanced by folding of the PEO chains leading to an effective increase in interfacial area between the blocks.

According to eq 2, a plot of $\log(L_c/N_2)$ as a function of $\log N_1$ should be linear, which is indeed observed with a slope of −0.34 (Figure 5). This is in excellent agreement with the prediction of DiMarzio et al. (slope −1/3).[49] From Figure 5 it becomes also apparent that the crystal thickness changes continuously with increasing block length rather than in a quantized manner, which indicates a continuous change in tilt angle.

4.3. Melting Point Depression (MPD). The melting temperature T_m of neat PEO ($M_n = 5000$ g/mol) did not change with crystallization temperature (Figure 6a). L_c values determined prior to melting scattered around a mean value of 29.8 nm. Thus, the equilibrium melting temperature of the PEO under investigation was taken as the mean value of the T_m obtained from DSC. The value of $T_m^0 = 62.1$ °C is in good agreement with the previously reported value of 61.6 °C for a PEO with $M_n = 5000$ g/mol.[83] Note that the value of 62.1 °C is the equilibrium melting temperature of the particular α-hydroxy-ω-methoxypoly(ethylene oxide) used in the present study and not the

dx.doi.org/10.1021/ma102867d |*Macromolecules* 2011, 44, 2953–2963

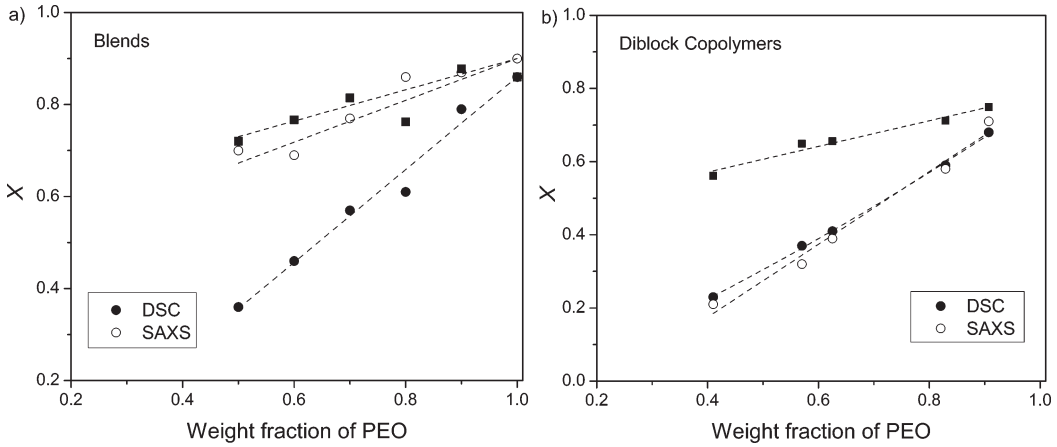

Figure 4. Degree of crystallinity, determined from DSC (●) and from SAXS (○), plotted as a function of composition for (a) PEO/PMA blends and (b) PEO-*b*-PMA diblock copolymers. The fractional crystallinity X'_{DSC} (■) of the PEO, i.e., DSC crystallinity divided by PEO weight fraction, is presented for comparison. Dashed lines are simple linear regressions.

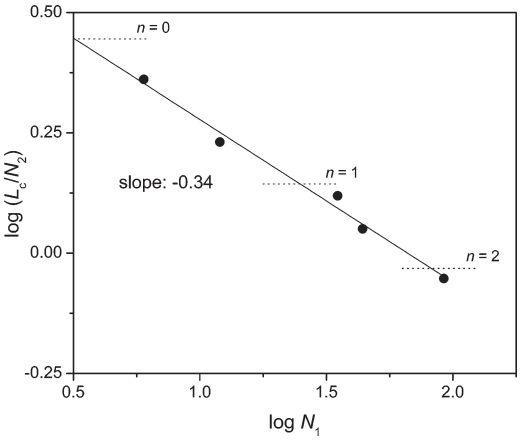

Figure 5. Double-logarithmic plot of lamella thickness L_c of diblock copolymers as a function of PMA block length as suggested by the scaling law given in eq 2. The dotted horizontal lines indicate the theoretical L_c of *n*-folded PEO chains with $N_2 = 114$ as calculated from eq 1. The continuous variation of *n* is an indication for chain tilting.

equilibrium melting temperature of PEO of infinite molar mass, which is generally accepted to be around 69 °C.[38,69] It should be mentioned that the macroinitiator used for block copolymer synthesis has a slightly lower T_m^0 of 61.8 °C. This slightly lower T_m^0 value compared to neat PEO is caused by the presence of the BIB end group. Such small shifts of melting points have also been reported for other PEOs with modified end groups.[84−86] Nevertheless, it is reasonable to state that the PEO in blends and the PEO in block copolymers are chemically identical species. Equilibrium melting points $T_{m,b}^0$ of the blends and diblock copolymers are determined using both extrapolation methods of Hoffman−Weeks and of Gibbs−Thomson. The corresponding plots are shown in Figures 6 and 7, respectively. Extrapolated equilibrium melting temperatures, slopes, and correlations of linear regressions are listed in Table 4.

Inspection of Figure 6, Figure 7, and Table 4 shows that the melting temperatures display indeed a linear dependence on $1/L_c$ and T_c, respectively. In contrast to neat low-molar-mass PEO homopolymers, a continuous thickening of the crystalline lamella without changing the fold number can be observed. In Figure 7 it is shown that the Hoffman−Weeks method leads approximately to an equilibrium melting temperature $T_{m,b}^0$ of an "ideal" crystal (i.e., untilted chains, smooth surface), but still being *n* times folded. If extended chain crystals are predominant, both methods differ in $T_{m,b}^0$ by only ∼2 K, as in case of the Hoffman−Weeks method the crystal has a finite thickness whereas in case of the Gibbs−Thomson procedure it has an infinite one. In the following, the Gibbs−Thomson approach is used since it allows also for conclusions on the surface free energy between crystal and amorphous surrounding (see eq 5).

From the slope *B* of eq 5, the surface free energy γ between crystal and amorphous layer can be calculated using $\Delta H_m^0 = 8668$ J/mol and a molar volume of the PEO repeat unit of $V_c = 36.1$ cm^3/mol. In case of the blends, γ was found to be independent of composition to a good approximation. The average value amounts to 23.8 mN/m (cf. Table 5). This value is within the limits discussed for extended chain crystals of α,ω-dihydroxy-PEO (between 11.1 and 26.3 mN/m).[38,69] Constancy of γ reveals that the crystal surface is not substantially altered by the presence of PMA in the blends. In contrast, γ is found to increase continuously with PMA content in the diblock copolymers up to a maximum value of 32.2 mN/m for PEO-*b*-PMA$_{53.8}$. This might be caused by an additional excess surface free energy contribution, resulting from the induced deformation of the PMA block, which is also responsible for the scaling behavior discussed above. An increase in γ with increasing length of the noncrystallizable block has also been observed in triblock copolymers of PEO and poly(propylene oxide), where PEO was the middle block.[87,88]

Figure 8 shows the equilibrium melting temperatures, determined using the Gibbs−Thomson approach, as a function of PMA volume fraction for both blends and diblock copolymers. The plot reveals that the MPD in diblock copolymers is much stronger as compared to the blends, especially for high PMA contents. For the blends, the Flory−Huggins interaction parameter χ can be determined from a plot of $(-\Delta H_m^0 / R(1/T_{m,b}^0 - 1/T_m^0) - A)$ over φ_1^2 as is shown in the inset of Figure 8. Linear regression yields an interaction parameter for the blends of $\chi = -0.04$. Within experimental error, it can thus be concluded that the system PEO/PMA has only weak attractive interactions. Unfortunately, eq 6 cannot be applied to diblock copolymers; i.e., a direct determination of χ for the diblock copolymers from the equilibrium melting temperatures is impossible.

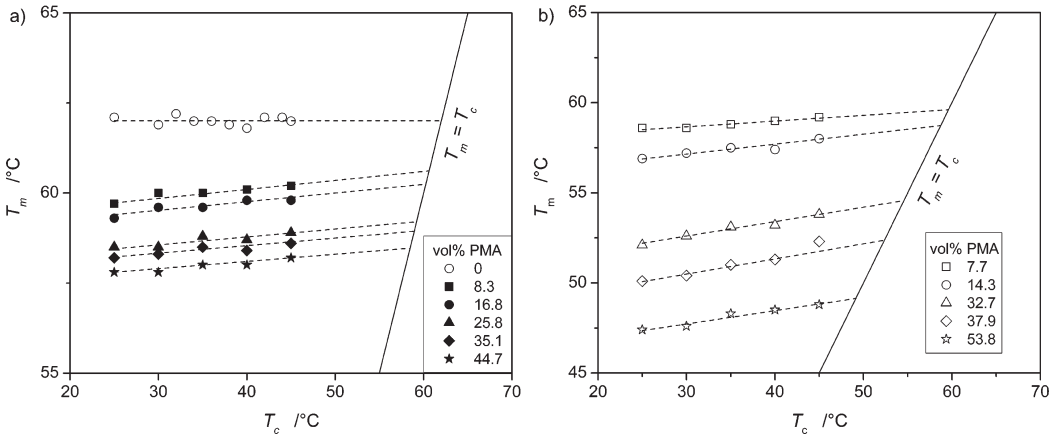

Figure 6. Hoffman–Weeks plots of (a) PEO/PMA blends and (b) PEO-*b*-PMA diblock copolymers. Solid lines indicate the equilibrium line given by $T_m = T_c$. The dotted lines present the linear regression.

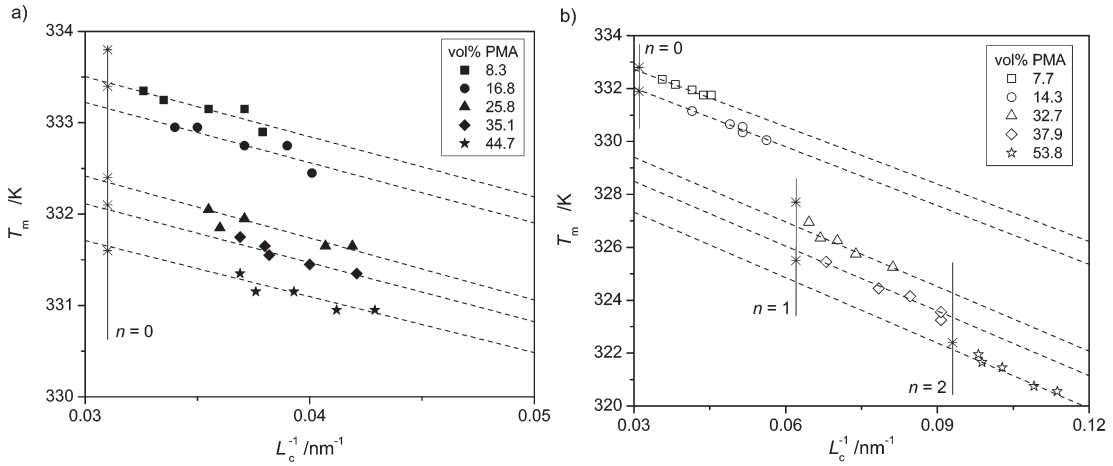

Figure 7. Gibbs–Thomson plots of (a) PEO/PMA blends and (b) PEO-*b*-PMA diblock copolymers. Dotted lines represent the linear regression. Vertical lines indicate the reciprocal length of an *n*-folded PEO chain and the asterisks the corresponding Hoffman–Weeks equilibrium melting temperatures.

Table 4. Equilibrium Melting Temperatures $T^0_{m,b}$ of Blends and Diblock Copolymers Determined Using Hoffman–Weeks and Gibbs–Thomson Extrapolation, Slope (B or α, See eqs 4 and 5), and Correlation R^2 of the Linear Regression

	Gibbs–Thomson, eq 5			Hoffman–Weeks, eq 4		
sample	$T^0_{m,b}$/K	B/nm^{-1}	R^2	$T^0_{m,b}$/K	α	R^2
PEO	335.3	0		335.3	0	
PEO/PMA$_{8.3}$	335.4	0.196	0.954	333.8	0.025	0.994
PEO/PMA$_{16.8}$	335.1	0.197	0.979	333.4	0.024	0.926
PEO/PMA$_{25.8}$	334.5	0.203	0.973	332.4	0.022	0.920
PEO/PMA$_{35.1}$	334.0	0.193	0.954	332.1	0.021	0.962
PEO/PMA$_{44.7}$	333.7	0.197	0.914	331.6	0.020	0.945
PEO-*b*-PMA$_{7.7}$	334.8	0.195	0.993	332.8	0.032	0.970
PEO-*b*-PMA$_{14.3}$	334.2	0.222	0.982	331.9	0.055	0.998
PEO-*b*-PMA$_{32.7}$	331.8	0.246	0.984	327.7	0.080	0.968
PEO-*b*-PMA$_{37.9}$	330.9	0.247	0.986	325.5	0.084	0.980
PEO-*b*-PMA$_{53.8}$	328.9	0.262	0.972	322.4	0.074	0.959

Table 5. Calculated Values of γ for Blends and Diblock Copolymers

blends	γ (mN/m)	copolymers	γ (mN/m)
PEO/PMA$_{8.3}$	23.6	PEO-*b*-PMA$_{7.7}$	23.5
PEO/PMA$_{16.8}$	23.7	PEO-*b*-PMA$_{14.3}$	26.8
PEO/PMA$_{25.8}$	24.5	PEO-*b*-PMA$_{32.7}$	29.9
PEO/PMA$_{35.1}$	23.3	PEO-*b*-PMA$_{37.9}$	30.1
PEO/PMA$_{44.7}$	23.8	PEO-*b*-PMA$_{53.8}$	32.2

Although χ is frequently assumed to be equal in blends and block copolymers composed of the same polymer species, there is experimental evidence that χ actually differs between binary blends and the respective diblock copolymers, but with the difference being rather small.[89] Such a small difference cannot account for the large MPD observed in case of the diblock copolymers. If it is assumed, however, that χ is equal for blends and diblock copolymers, the only parameter which can be responsible for the large MPD difference is the entropy of melting. A possible explanation might be that the strong stretching of the PMA chains leads to an entropy gain during melting

dx.doi.org/10.1021/ma102867d |*Macromolecules* 2011, 44, 2953–2963

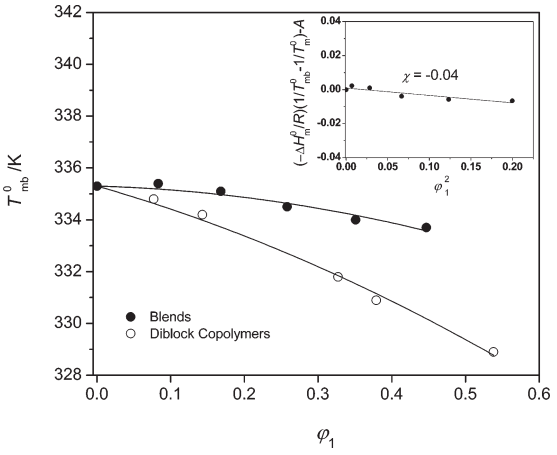

Figure 8. Depression of the equilibrium melting temperatures (determined by Gibbs−Thomson approach) of PEO/PMA blends (●) and PEO-*b*-PMA diblock copolymers (○). Solid lines are second-order polynomial regressions. The inset shows a plot of quantity $(-\Delta H^0_m / R(1/T^0_{m,b} - 1/T^0_{m,b}) - A)$ as a function of ${\varphi_1}^2$ to determine the interaction parameter χ in PEO/PMA blends.

which is larger as compared to the respective blends. Assuming constant enthalpy of melting, this would lead to a stronger decrease in the equilibrium melting temperature.

5. CONCLUSION

A study comparing the crystallization behavior of a miscible polymer blend and the respective diblock copolymers was carried out. The blends were prepared by mixing the homopolymers PEO and PMA, whereas the diblock copolymers were synthesized by ATRP using an identical PEO species as macroinitiator for the addition of the PMA block. Crystallization and melting behavior of blends and diblock copolymers was studied by TR-SAXS and DSC. From TR-SAXS measurements it was concluded that neat PEO and PEO in the blends crystallized at 40 °C into crystals having once-folded chains owing to crystallization kinetics. The crystals thickened upon heating to approach extended chains. The long period d, determined close to the melting temperature, slightly increased with PMA content, whereas the lamella thickness L_c slightly decreased. From crystallinities X_{DSC} and X_{SAXS}, it was found that a large fraction of PMA is excluded from the amorphous region between the lamellae. Crystallization behavior was entirely different in diblock copolymers PEO-*b*-PMA. Here, PEO chains had several folds when crystallized, with the fold number being increased with PMA block length. Upon heating, thickening of the lamellae was observed as well, but with restrictions. At a certain PMA block length, thickening to extended chains did no longer occur. This was attributed to the influence of the covalently bound PMA block, which significantly hampered the formation of extended chain crystals, especially when the PMA block became sufficiently large. The equilibrium decrease of lamella thickness L_c as a function of the degree of polymerization N_1 of the PMA blocks was successfully described by the scaling law $L_c \propto N_2 {N_1}^{-1/3}$.

The equilibrium melting temperatures of blends and diblock copolymers were determined using both the Hoffman−Weeks and the Gibbs−Thomson extrapolation methods. It was found, that the Hoffman−Weeks approach seems to extrapolate to the maximum thickness of a crystal with defined fold number, whereas Gibbs−Thomson extrapolates to infinite crystal thickness irrespective of fold number. The equilibrium melting temperatures determined for the blends according to Gibbs−Thomson allowed determination of the interaction parameter χ. It was shown that the depression of equilibrium melting temperature in diblock copolymers is much larger compared to the blends.

■ ASSOCIATED CONTENT

Ⓢ Supporting Information. Calculation of volume fraction is described in more detail, figures showing the one-dimensional electron density correlation function of the diblock copolymer PEO-*b*-$PMA_{7.7}$, and TR-SAXS traces of the samples PEO-*b*-$PMA_{14.3}$ and PEO-*b*-$PMA_{37.9}$. This material is available free of charge via the Internet at http://pubs.acs.org.

■ AUTHOR INFORMATION

Corresponding Author

*E-mail: joerg.kressler@chemie.uni-halle.de.

■ ACKNOWLEDGMENT

J.K. thanks Deutsche Forschungsgemeinschaft (FO 1145).

■ REFERENCES

(1) Krause, S.; Goh, S. H. In *Polymer Blends Handbook*; Utracki, L. A., Ed.; Kluwer Academic Publishers: Dordrecht, 2002; Vol. 2, p 1242.
(2) Pedemonte, E.; Burgisi, G. *Polymer* **1994**, *35*, 3719–3721.
(3) Pfefferkorn, D.; Sonntag, S.; Kyerematen, S. O.; Funke, Z.; Kammer, H.-W.; Kressler, J. *J. Polym. Sci., Part B: Polym. Phys.* **2010**, *48*, 1893–1900.
(4) Flory, P. J. In *Principles of Polymer Chemistry*, 2nd ed.; Cornell University Press: Ithaca, NY, 1957; p 568.
(5) Morra, B. S.; Stein, R. S. *J. Polym. Sci., Polym. Phys. Ed.* **1982**, *20*, 2243–2259.
(6) Plans, J.; MacKnight, W. J.; Karasz, F. E. *Macromolecules* **1984**, *17*, 810–814.
(7) Kressler, J.; Kammer, H.-W. *Polym. Bull.* **1988**, *19*, 283–288.
(8) Nishi, T.; Wang, T. T. *Macromolecules* **1975**, *8*, 909–915.
(9) Galin, M.; Mathis, A. *Macromolecules* **1981**, *14*, 677–683.
(10) Unger, R.; Beyer, D.; Donth, E. *Polymer* **1991**, *32*, 3305–3312.
(11) Ishikawa, S. *Eur. Polym. J.* **1993**, *29*, 1621–1624.
(12) Yang, Y. W.; Tanodekaew, S.; Mai, S. M.; Booth, C.; Ryan, A. J.; Bras, W.; Viras, K. *Macromolecules* **1995**, *28*, 6029–6041.
(13) Mai, S. M.; Fairclough, J. P. A.; Viras, K.; Gorry, P. A.; Hamley, I. W.; Ryan, A. J.; Booth, C. *Macromolecules* **1997**, *30*, 8392–8400.
(14) Shiomi, T.; Tsukada, H.; Takeshita, H.; Takenaka, K.; Tezuka, Y. *Polymer* **2001**, *42*, 4997–5004.
(15) Hong, S.; Yang, L.; MacKnight, W. J.; Gido, S. P. *Macromolecules* **2001**, *34*, 7009–7016.
(16) Hamley, I. *Adv. Polym. Sci.* **1999**, *148*, 113–137.
(17) Müller, A. J.; Balsamo, V.; Arnal, M. L. *Adv. Polym. Sci.* **2005**, *190*, 1–63.
(18) Nandan, B.; Hsu, J. Y.; Chen, H. L. *Polym. Rev.* **2006**, *46*, 143–172.
(19) Nojima, S.; Ono, M.; Ashida, T. *Polym. J.* **1992**, *24*, 1271–1280.
(20) Rangarajan, P.; Register, R. A.; Fetters, L. J. *Macromolecules* **1993**, *26*, 4640–4645.
(21) Rangarajan, P.; Register, R. A.; Adamson, D. H.; Fetters, L. J.; Bras, W.; Naylor, S.; Ryan, A. J. *Macromolecules* **1995**, *28*, 1422–1428.
(22) Richardson, P. H.; Richards, R. W.; Blundell, D. J.; MacDonald, W. A.; Mills, P. *Polymer* **1995**, *36*, 3059–3069.

(23) Lee, L. B. W.; Register, R. A. *Macromolecules* **2004**, *37*, 7278–7284.
(24) Shin, D.; Shin, K.; Aamer, K. A.; Tew, G. N.; Russell, T. P. *Macromolecules* **2005**, *38*, 104–109.
(25) He, C.; Sun, J.; Ma, J.; Chen, X.; Jing, X. *Biomacromolecules* **2006**, *7*, 3482–3489.
(26) Hoffman, J. D.; Weeks, J. J. *J. Res. Natl. Bur. Stand.* **1962**, *66A*, 13–28.
(27) Wunderlich, C. In *Crystal Melting. Macromolecular Physics*; Academic Press: New York, 1980.
(28) Arlie, J. P.; Spegt, P.; Skoulios, A. E. *Makromol. Chem.* **1966**, *99*, 160–174.
(29) Godovsky, Y. K.; Slonimsky, G. L.; Garbar, N. M. *J. Polym. Sci., Part C: Polym. Symp.* **1972**, *38*, 1–21.
(30) Arlie, J. P.; Spegt, P.; Skoulios, A. E. *Makromol. Chem.* **1967**, *104*, 212–229.
(31) Spegt, P. *Macromol. Chem.* **1970**, *139*, 139–152.
(32) Spegt, P. *Makromol. Chem.* **1970**, *140*, 167–177.
(33) Cheng, S. Z. D.; Zhang, A.; Barley, J. S.; Chen, J. *Macromolecules* **1991**, *24*, 3937–3944.
(34) Cheng, S. Z. D.; Chen, J.; Barley, J. S.; Zhang, A. *Macromolecules* **1992**, *25*, 1453–1460.
(35) Song, K.; Krimm, S. *Macromolecules* **1990**, *23*, 1946–1957.
(36) Kim, I.; Krimm, S. *J. Polym. Sci., Part B: Polym. Phys.* **1997**, *35*, 1117–1126.
(37) Kovacs, A. J.; Gonthier, A. *Kolloid Z. Z. Polym.* **1972**, *250*, 530–551.
(38) Buckley, C. P.; Kovacs, A. J. *Colloid Polym. Sci.* **1976**, *254*, 695–715.
(39) Tang, X. F.; Wen, X. J.; Zhai, X. M.; Xia, N.; Wang, W.; Wegner, G.; Wu, Z. H. *Macromolecules* **2007**, *40*, 4386–4388.
(40) Zhai, X. M.; Wang, W.; Ma, Z. P.; Wen, X. J.; Yuan, F.; Tang, X. F.; He, B. *Macromolecules* **2005**, *38*, 1717–1722.
(41) Zhai, X. M.; Zhang, G. L.; Ma, Z. P.; Tang, X. F.; Wang, W. *Macromol. Chem. Phys.* **2007**, *208*, 651–657.
(42) Liu, Y.-X.; Li, J.-F.; Zhu, D.-S.; Chen, E.-Q.; Zhang, H.-D. *Macromolecules* **2009**, *42*, 2886–2890.
(43) Takahashi, Y.; Tadokoro, H. *Macromolecules* **1973**, *6*, 672–675.
(44) Rastogi, S.; Spoelstra, A. B.; Goosens, J. G. P.; Lemstra, P. J. *Macromolecules* **1997**, *30*, 7880–7889.
(45) Dreyfuss, P.; Keller, A. *J. Macromol. Sci., Part B: Phys.* **1970**, *B4*, 811–836.
(46) Kawaguchi, A.; Murakami, S.; Kajiwara, K.; Katayama, K.-I.; Nerger, D. *J. Polym. Sci., Part B: Polym. Phys.* **1989**, *27*, 1463–1476.
(47) Sawayanagi, T.; Tanaka, T.; Iwata, T.; Abe, H.; Doi, Y.; Ito, K.; Fujisawa, T.; Fujita, M. *Macromolecules* **2006**, *39*, 2201–2208.
(48) Fujita, M.; Sawayanagi, T.; Abe, H.; Tanaka, T.; Iwata, T.; Ito, K.; Fujisawa, T.; Maeda, M. *Macromolecules* **2008**, *41*, 2852–2858.
(49) DiMarzio, E. A.; Guttman, C. M.; Hoffman, J. D. *Macromolecules* **1980**, *13*, 1194–1198.
(50) Whitmore, M. D.; Noolandi, J. *Macromolecules* **1988**, *21*, 1482–1496.
(51) Alamo, R. G.; Viers, B. D.; Mandelkern, L. *Macromolecules* **1995**, *28*, 3205–3213.
(52) Kressler, J.; Svoboda, P.; Inoue, T. *Polymer* **1993**, *34*, 3225–3233.
(53) Xu., J.; Bellas, V.; Jungnickel, B.; Stühn, B.; Rehahn, M. *Macromol. Chem. Phys.* **2010**, *211*, 1261–1271.
(54) Marand, H.; Xu, J.; Srinivas, S. *Macromolecules* **1998**, *31*, 8219–8229.
(55) Schmidtke, J.; Strobl, G.; Thurn-Albrecht, T. *Macromolecules* **1997**, *30*, 5804–5821.
(56) Hauser, G.; Schmidtke, J.; Strobl, G. *Macromolecules* **1998**, *31*, 6250–6258.
(57) Heck, B.; Hugel, T.; Iijima, M.; Sadiku, E.; Strobl, G. *New J. Phys.* **1999**, *1*, 17.1–17.29.
(58) Al-Hussein, M.; Strobl, G. *Macromolecules* **2002**, *35*, 1672–1676.
(59) Heck, B.; Hugel, T.; Iijima, M.; Strobl, G. *Polymer* **2000**, *41*, 8839–8848.
(60) Strobl, G. *Prog. Polym. Sci.* **2006**, *31*, 398–442.
(61) Flory, P. J.; Vrij, A. *J. Am. Chem. Soc.* **1963**, *85*, 3548–3553.
(62) Rostami, S. D. *Eur. Polym. J.* **2000**, *36*, 2285–2290.
(63) Rim, P. B.; Runt, J. P. *Macromolecules* **1984**, *17*, 1520–1526.
(64) Chow, T. S. *Macromolecules* **1990**, *23*, 333–337.
(65) Höhne, G. W. H. *Polymer* **2002**, *43*, 4689–4698.
(66) Höhne, G. W. H. *Thermochim. Acta* **2003**, *403*, 26–36.
(67) Yamada, K.; Hikosaka, M.; Toda, A.; Yamazaki, S.; Tagashira, K. *Macromolecules* **2003**, *36*, 4790–4801.
(68) Strobl, G.; Schneider, M. *J. Polym. Sci., Polym. Phys. Ed.* **1980**, *18*, 1343–1359.
(69) Buckley, C. P.; Kovacs, A. J. *Prog. Colloid Polym. Sci.* **1975**, *58*, 44–52.
(70) Takeshita, H.; Gao, Y.-J.; Takata, Y.; Takenaka, K.; Shiomi, T.; Wu, C. *Polymer* **2010**, *51*, 799–806.
(71) Mani, S.; Weiss, R. A.; Hahn, S. F.; Williams, C. E.; Cantino, M. E.; Khairallah, L. H. *Polymer* **1998**, *39*, 2023–2033.
(72) Förster, S.; Timmann, A.; Konrad, M.; Schellbach, C.; Meyer, A.; Funari, S. S.; Mulvaney, P.; Knott, R. *J. Phys. Chem. B* **2005**, *109*, 1347–1360.
(73) Hamley, I.; Castelletto, V. In *Soft Mater Characterization*, 1st ed.; Borsali, R., Pecora, R., Eds.; Springer: New York, 2008; Vol. 2, pp 1023−1081.
(74) Talibuddin, S.; Wu, L.; Runt, J.; Lin, J. S. *Macromolecules* **1996**, *29*, 7527–7535.
(75) Talibuddin, S.; Runt, J.; Liu, L. Z.; Chu, B. *Macromolecules* **1998**, *31*, 1627–1634.
(76) Lisowski, M. S.; Liu, Q.; Cho, J.; Runt, J.; Yeh, F.; Hsiao, B. S. *Macromolecules* **2000**, *33*, 4842–4849.
(77) Shieh, Y.-T.; Lin, Y.-G.; Chen, H.-L. *Polymer* **2002**, *43*, 3691–3698.
(78) Fragiadakis, D.; Runt, J. *Macromolecules* **2010**, *43*, 1028–1034.
(79) Warner, F. P.; MacKnight, W. J.; Stein, R. S. *J. Polym. Sci., Polym. Phys. Ed.* **1977**, *15*, 2113–2126.
(80) Russell, T. P.; Ito, H.; Wignall, G. D. *Macromolecules* **1988**, *21*, 1703–1709.
(81) Russell, T. P.; Stein, R. S. *J. Polym. Sci., Polym. Phys. Ed.* **1983**, *21*, 999–1010.
(82) Wang, C.; Thomann, R.; Kressler, J.; Thomann, Y.; Crämer, K.; Stühn, B.; Svoboda, P.; Inoue, T. *Acta Polym.* **1997**, *48*, 354–362.
(83) Qiu, W.; Pyda, M.; Nowak-Pyda, E.; Habenschuss, A.; Wunderlich, B. *Macromolecules* **2005**, *38*, 8454–8467.
(84) Booth, C.; Bruce, J. M.; Buggy, M. *Polymer* **1972**, *13*, 475–478.
(85) Fraser, M. J.; Cooper, D. R.; Booth, C. *Polymer* **1977**, *18*, 852–854.
(86) Cheng, S. Z. D.; Wu, S. S.; Chen, J.; Zhuo, Q.; Quirk, R. P.; von Meerwall, E. D.; Hsiao, B. S.; Habenschuss, A.; Zschack, P. R. *Macromolecules* **1993**, *26*, 5105–5117.
(87) Booth, C.; Pickles, C. J. *J. Polym. Sci., Polym. Phys. Ed.* **1973**, *11*, 249–264.
(88) Ashman, P. C.; Booth, C.; Cooper, D. R.; Price, C. *Polymer* **1975**, *16*, 897–902.
(89) Maurer, W. W.; Bates, F. S.; Lodge, T. P.; Almdal, K.; Mortensen, K.; Fredrickson, G. H. *J. Chem. Phys.* **1998**, *108*, 2989–3000.